Supporting Information

High Performance Potassium-Sulfur Batteries and Its Reaction Mechanism

Xinxin Zhao,[a] Youran Hong,[b] Mingren Cheng,[a] Shiwen Wang,[c] Lei Zheng,[d] Jiangwei Wang,[b]* Yunhua Xu[a,e]*

[a]School of Materials Science and Engineering, Key Laboratory of Advanced Ceramics and Machining Technology (Ministry of Education), Tianjin Key Laboratory of Composite and Functional Materials, Tianjin University, Tianjin 300072, China.
E-mail: yunhua.xu@tju.edu.cn

[b]Center of Electron Microscopy and State Key Laboratory of Silicon Materials, School of Materials Science and Engineering, Zhejiang University, Hangzhou 310027, China.

[c]College of Materials and Chemical Engineering, Zhengzhou University of Light Industry, Zhengzhou 450001, China.

[d]Beijing Synchrotron Radiation Facility, Institute of High Energy Physics, Chinese Academy of Sciences, Beijing 100049, China.

[e]Collaborative Innovation Center of Chemical Science and Engineering (Tianjin), Tianjin 300072, China.

Keywords: potassium-sulfur battery, small-molecule sulfur cathode, free-standing electrode, high energy density, electrospun carbon fiber

Experimental Section

Preparation of PCNF mat

The free-standing PCNF mat was prepared using an versatile electrospinning process, followed by a carbonization treatment. Typically, polyacrylonitrile (PAN, MW = 150,000 g mol^{-1}, J&K, 1.0 g) was dissolved in N,N-dimethylformamide (DMF, > 99.5%, Titan, 10 mL) followed by magnetic stirring at 80 °C overnight to form an viscous and homogeneous solution. The obtained solution was loaded into a 5 mL plastic syringe with a 21-gauge blunt tip needle. Electrospinning process was then carried out by applying an voltage of 15 kV on the needle with a flow rate of 0.8 mL h^{-1}. The polymer fiber mat was collected using a grounded roller with a distance of 14 cm to the syringe needle. The collected PAN mat was firstly stabilized at 280 °C for 3 hours in air with a heating rate of 2 °C min^{-1} followed by carbonization at a high temperature of 800 °C for 2 hours with a heating rate of 5 °C min^{-1} under nitrogen atmosphere, donated as PCNF-800. Finally, the resultant carbon fiber mat was treated at 350 °C in air for 2 hours, and the PCNF mat was obtained.

Preparation of PCNF/S composite

The mixture of bulk sulfur (cyclo-S_8) (99.5%, Alfa Aesar) and the PCNF mat in a mass ratio (3:1) was sealed into glass tube under vacuum and heated at 500 °C for 5 hours with a heating ramp of 5 °C min^{-1}. The resulting product was then heated at 200 °C for 4 hours in argon atmosphere with a heating rate of 2 °C min^{-1} to remove the superficial sulfur and finally free-standing microporous carbon nanofiber/small-molecule sulfur (PCNF/S) composite was obtained with a sulfur loading of 0.5-1.0 mg cm^{-2}.

Materials and structural characterizations

Morphological characterizations of the PCNF and PCNF/S composite mats were carried out on field-emission scanning electron microscopy (FESEM, Hitachi, S-4800) and transmission electron microscopy (TEM, JEOL, JEM-2100F). Both SEM and TEM energy dispersive X-ray spectroscopy (EDS) were performed on Oxford energy spectrometer. X-ray diffraction (XRD)

patterns were collected on Rigaku Ultima IV with Cu Kα radiation source (V = 40 kV, I = 40 mA and λ = 1.5418 Å). Raman spectra were collected using a laser wavelength of 532 nm on a Renishaw InVIA Reflex Raman microspectrometer. X-ray photoelectron spectroscopy (XPS) measurement was performed on a Thermo Scientific K-Alpha X-ray photoelectron spectrometer with mono Al Kα radiation at room temperature. The microporous structure of the PCNF and PCNF/S composite mats was analyzed using CO_2 adsorption-desorption on a ASAP 2420-4 volumetric adsorption analyzer (Micromeritics). The pore size distribution was calculated using nonlocalized DFT method, and the pore volume was obtained using Horvath-Kawazoe method. The thermal stability of bulk cyclo-S_8 and the PCNF/S composite was investigated using a thermo-gravimetric analysis (TGA, TA, Q50) in nitrogen with a heating rate of 10 °C min^{-1}. Element analysis was applied on Elementar, Vario Micro Cube. The Fourier transform infrared spectroscopy (FTIR) spectra were recorded using KBr pellets on a Bruker Alpha spectrometer. The UV-vis samples were prepared by collecting the electrolytes from the disassembled batteries and the data were conducted on Jindao UV-3600 plus.

Electrochemical characterization

The free-standing PCNF/S composites were directly used as working electrodes (~7 mm×7 mm) with the weight of 1-2 mg to assemble CR2032-type coin cells in an argon-filled glove box (H_2O, O_2 < 0.1 ppm). Potassium metal (K, 99.5%, Sigma-Aldrich) was used as counter and reference electrode and Celgard®2400 (Celgard, LLC Corp.) as separator. The K metal anode used in this work is ~6 mm*6 mm in size, ~300-500 μm in thickness with a mass of ~12 mg. 50 μL 1.0 M potassium bis(fluoroslufonyl)imid (KFSI)-dimethoxyethane (DME) and 0.8 M potassium hexafluorophosphate (KPF_6) in ethylene carbonate (EC)/diethyl carbonate (DEC) (1:1 by volume) were used as electrolytes.

The galvanostatic charge/discharge performance of the half-cells was tested on a LAND CT-2001A (Wuhan) instrument in an voltage range of 0.5-3.0 V (vs. K^+/K) at ambient temperature. Cyclic voltammetry (CV) curves were carried out on CHI660E electrochemical test station at a

scan rate of 0.02 mV s^{-1} in the range 0.5-3.0 V. A Solartron electrochemical workstation (1400+1470) was employed for electrochemical impedance spectrometry (EIS) test in the frequency range of 0.01 Hz to 1 MHz with an ac amplitude of 5 mV.

In order to rule out the influence of element sulfur in the salt of KFSI, 0.8 M KPF_6 in EC/DEC (1:1) was applied for SEM, TEM, *ex-situ* XPS and sulfur K-edge XANES measurements. In addition, all the batteries were potassiated and depotassiated to desired voltages and then kept for 6 hours. The potassiated/depotassiated PCNF/S composite electrodes were retrieved and rinsed with DEC solvent several times to remove residual electrolyte before analysis.

For the *ex-situ* XPS depth-profile test, the PCNF/S composite electrodes were potassiated and depotassiated to desired voltages at 20 mA g^{-1}. The washed electrodes were sealed in a tightly-closed XPS sample holder in an argon-filled glove box and then transferred into the XPS test chamber without exposure to air. The profiles were obtained after a 20 s etching process with a rate of 0.32 nm s^{-1}.

TOF-SIMS measurement

The time-of-flight secondary ion mass spectrometry (TOF-SIMS) analysis was conducted on a TOF-SIMS 5 spectrometer (ION-TOF GmbH, 2015). The spectrometer was run at an operating pressure below 1×10^{-9} mbar. Bi^{3+} primary ion clusters at 60 keV were employed on a 200 × 200 μm^2 area. Sputtering process was done using a 10 keV Ar^+ beam with an etching rate of 0.214 nm s^{-1} and SiO_2 as reference. Data acquisition and post-processing analyses were performed using Software Surface Lab. Both positive and negative ion profiles were recorded and analyzed. The intensity reported used a logarithmic scale in order to magnify the low-intensity signals.

Sulfur K-edge XANES spectroscopy analysis

The sulfur K-edge X-ray absorption near-edge structure (sulfur K-edge XANES) data of the PCNF/S composite electrodes at different potassiated/depotassiated states were collected in partial fluorescence yield mode at beamline 4B7A of Beijing Synchrotron Radiation Facility

(BSRF). The incoming X-ray beam was monochromatized by a fixed-exit Si (111) double-crystal monochromator. Monocharomator energy was calibrated against the peak of the white line of K_2SO_4 at 2.4824 keV. Furthermore, to establish a relationship between the edge energy and oxidation state, bulk sulfur (cyclo-S_8) and phenyl disulfide were applied as reference materials. For sample preparation, the reference materials and PCNF/S composite electrodes were neatly pressed onto conductive double sided carbon adhesive tape in an argon-filled glove box to avoid the side reactions with oxygen and humidity. All of the raw XANES spectra were processed using Athena software package.

The calculation of energy density

The energy density value *E* (Wh/kg) calculation process was showed as follows:

$$E = C_{d\text{-}total} * V_d \quad (1)$$

Where $C_{d\text{-}total}$ represents the discharge capacity based on the total weight including active material, binder and conductive agents, V_d represents the average discharge voltage.

$$C_{d\text{-}total} = (C_d * m_{active})/(m_{total} + m_{collector}) \quad (2)$$

Where C_d represents the discharge capacity obtained from the literature, m_{active} represents the weight of active electrode material, m_{total} represents the total weight of the electrode including active electrode material, binder and conductive agents, and $m_{collector}$ represents the mass of the current collectors.

$$m_{active} = L_{active} * A_{electrode} \quad (3)$$

$$m_{total} = m_{active}/w \quad (4)$$

$$m_{collector} = L_{collector} * A_{electrode} \quad (5)$$

Where L_{active} represents the area loading of the active materials, $A_{electrode}$ represents the area of the electrode, and w represents the mass percentage of active material in the electrode. (The L_{active}, $L_{collector}$, and $A_{electrode}$ were set to be 1 mg cm^{-2}, 5 mg cm^{-2} and 1cm^2, respectively, when the values were not provided in the literature.)

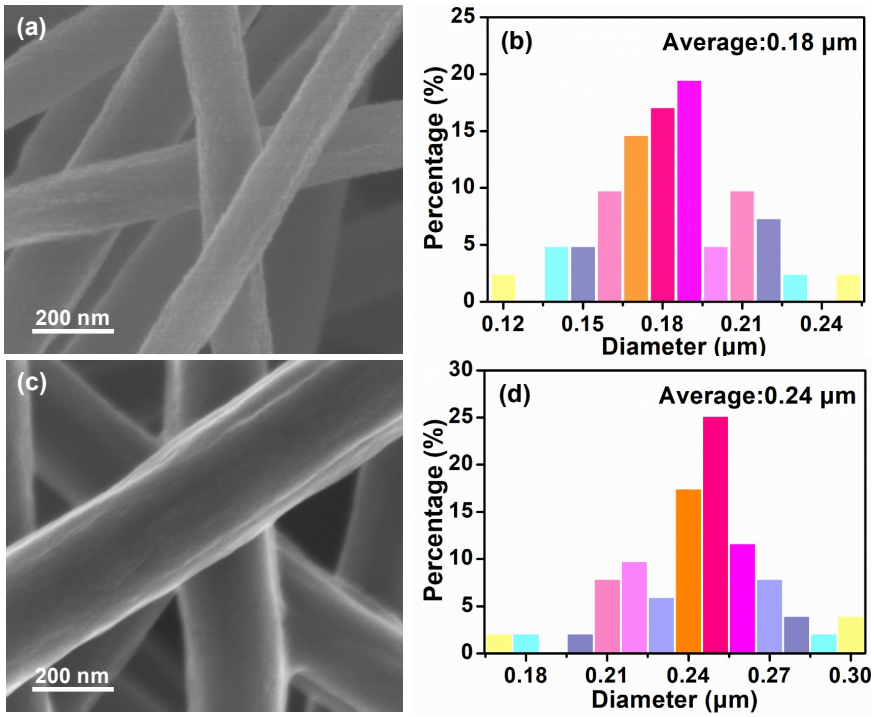

Figure S1. (a,c) SEM images and (b,d) diameter distribution of the (a,b) PCNF mat and (c,d) PCNF/S composite.

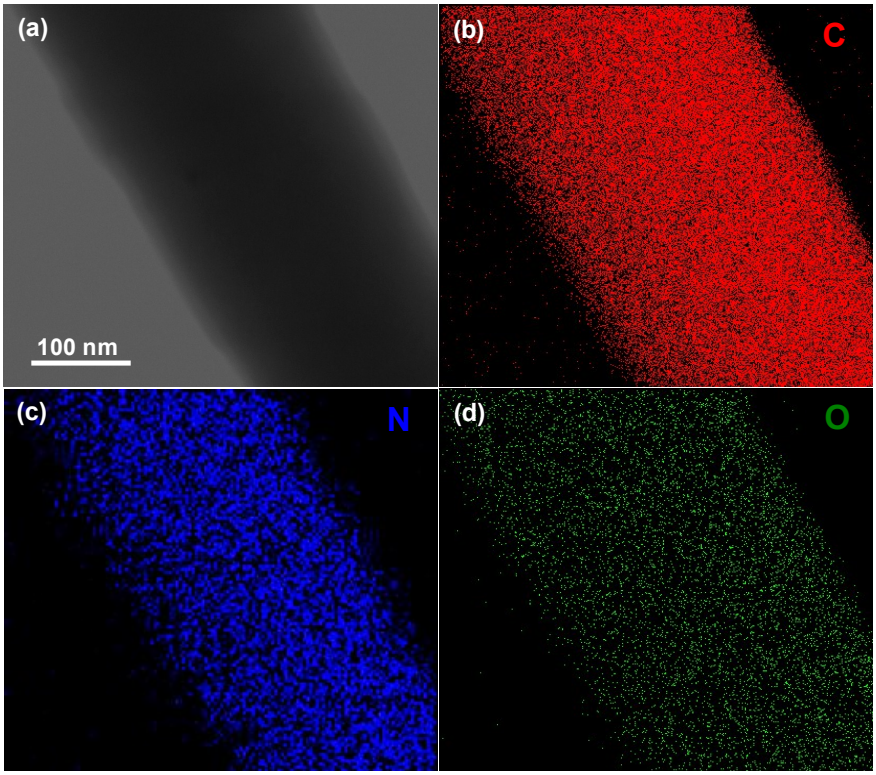

Figure S2. (a) Light-field image and EDS element mapping images of (b) C, (c) N and (d) O of the PCNF/S composite.

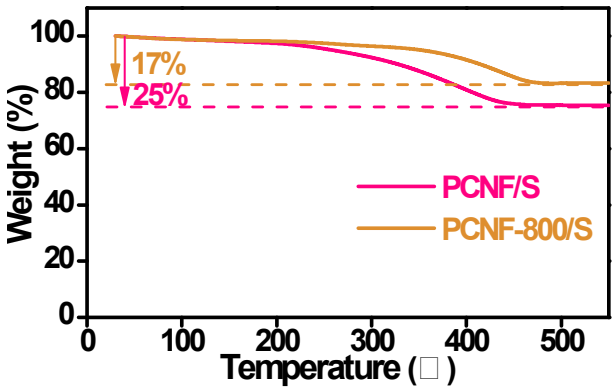

Figure S3. TGA curves of PCNF/S and PCNF-800/S composites.

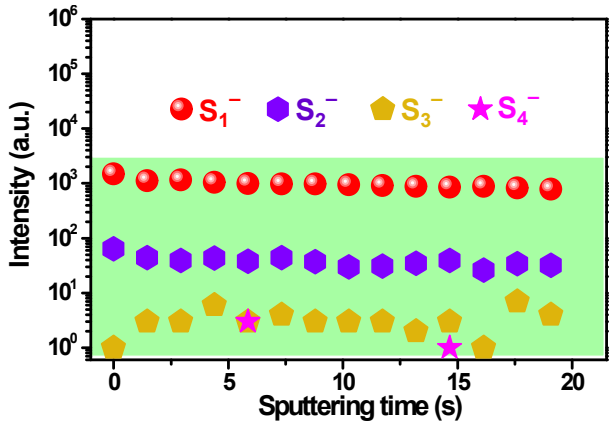

Figure S4. The second sputtering process under negative ion sputtering of the PCNF/S composite.

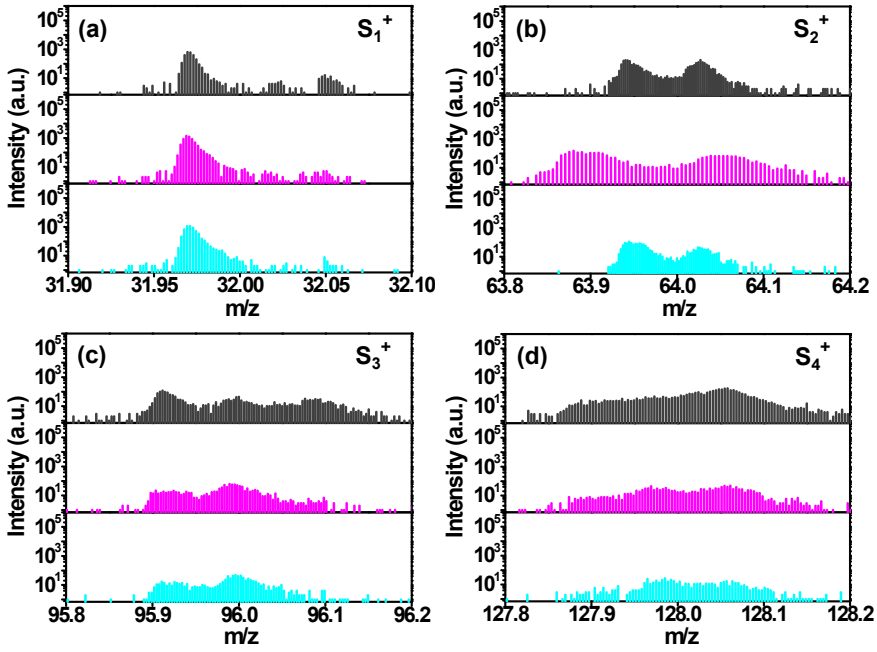

Figure S5. Positive ion mass spectra of TOF-SIMS analysis of the PCNF/S composite: (a) S_1^+, (b) S_2^+, (c) S_3^+ and (d) S_4^+. The black curves are on the pristine surface, the pinks are the curves after the first sputtering and the light blues are those after second sputtering process, respectively.

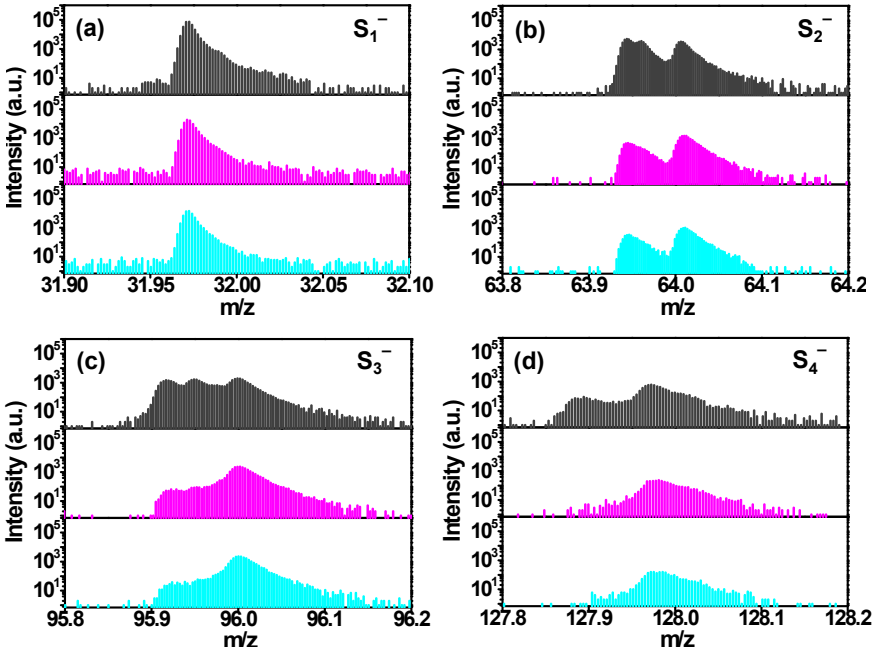

Figure S6. Negative ion mass spectra of TOF-SIMS analysis of the PCNF/S composite: (a) S_1^-, (b) S_2^-, (c) S_3^- and (d) S_4^-. The black curves are on the pristine surface, the pinks are the curves

after the first sputtering and the light blues are those after second sputtering process, respectively.

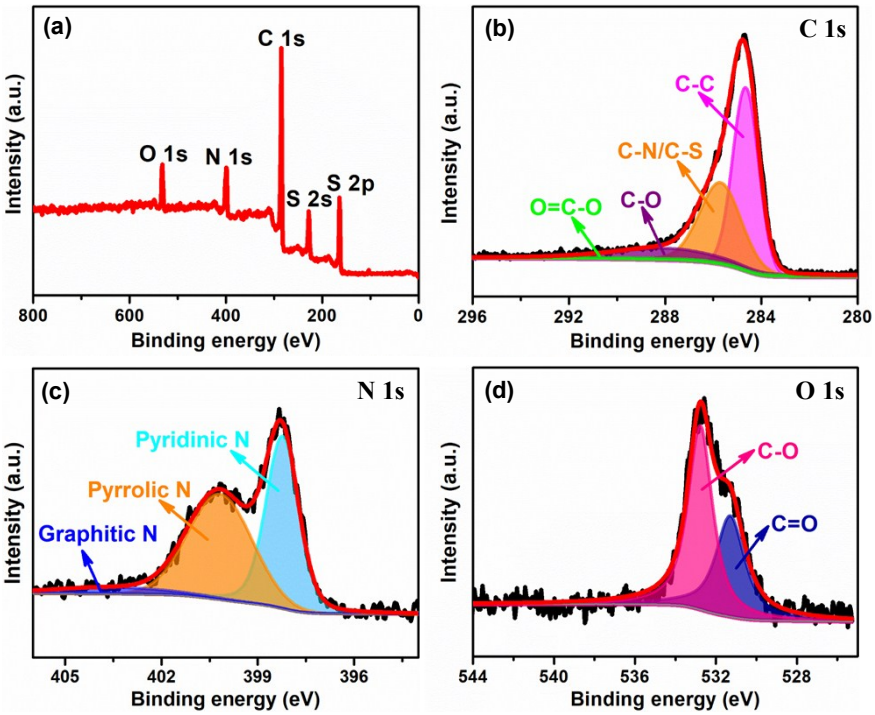

Figure S7. Chemical property characterization of the PCNF/S composite: (a) XPS survey and high-resolution XPS spectra of (b) C 1s, (c) N 1s and (d) O 1s, respectively.

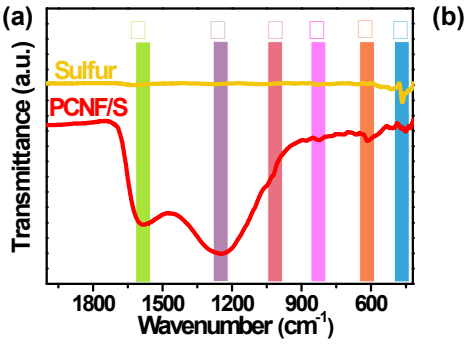

(b)

Order number	Wavenumber (cm^{-1})	Assignments
I	465	S-S Stretch
II	616	C-S stretch
III	832	ring breathing of hexahydric-rings in the main-chain
IV	1015	ring breath, containing a C-S bond in the side-chain
V	1256	C=N stretch
VI	1585	C=C stretch

Figure S8. Chemical property characterization of the PCNF/S composite: (a) FTIR spectra of bulk sulfur and the PCNF/S composite and (b) summary of FTIR peaks and assignments.

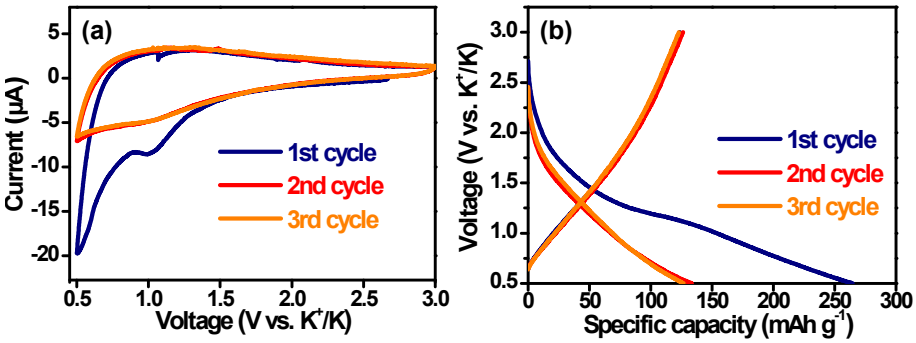

Figure S9. Electrochemical performance of the PCNF electrodes with the electrolyte of 1.0 M KFSI in DME: (a) CV curves at a scan rate of 0.05 mV s^{-1}, (b) galvanostatic charge/discharge profiles at 20 mA g^{-1}.

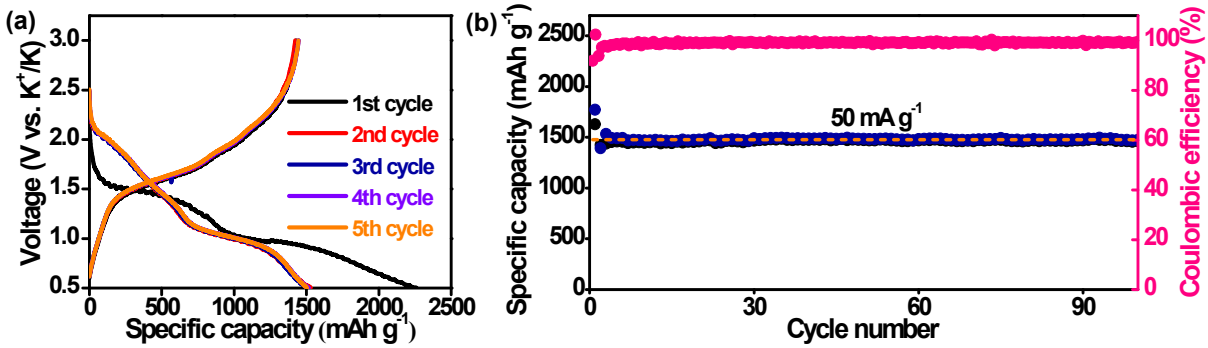

Figure S10. Electrochemical performance of the PCNF/S composite electrodes in the voltage window of 0.5-3.0 V with the electrolyte of 0.8 M KPF_6 in EC/DEC: (a) galvanostatic charge/discharge profiles in the first five cycles at 20 mA g^{-1} and (b) cycling stability at 50 mA g^{-1}.

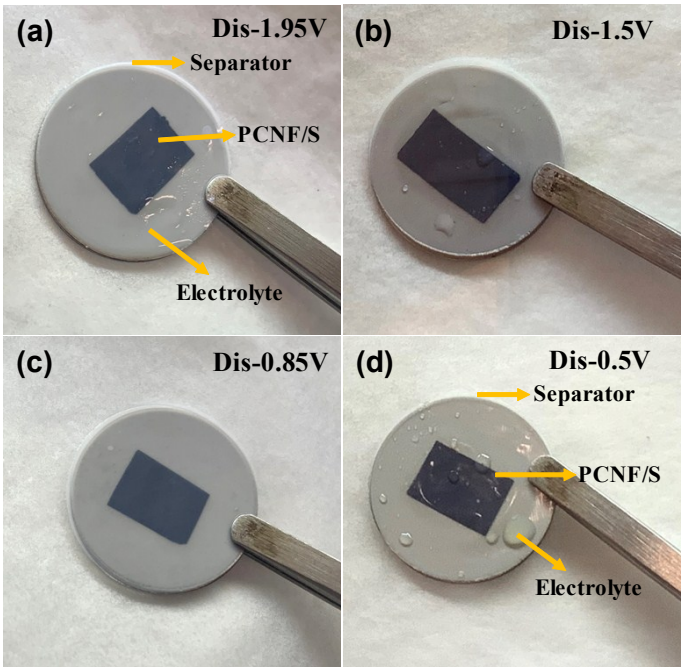

Figure S11. Optical photographs of PCNF/S composite electrodes after disassembling the batteries at different potassiation states in the electrolyte of 0.8 M KPF_6 in EC/DEC.

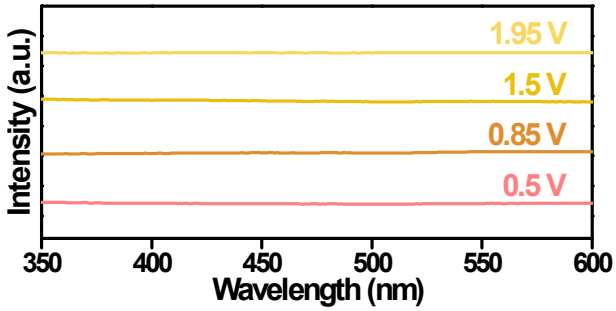

Figure S12. UV-vis spectra of electrolytes collected from the disassembled batteries at different discharge states in the electrolyte of 0.8 M KPF_6 in EC/DEC.

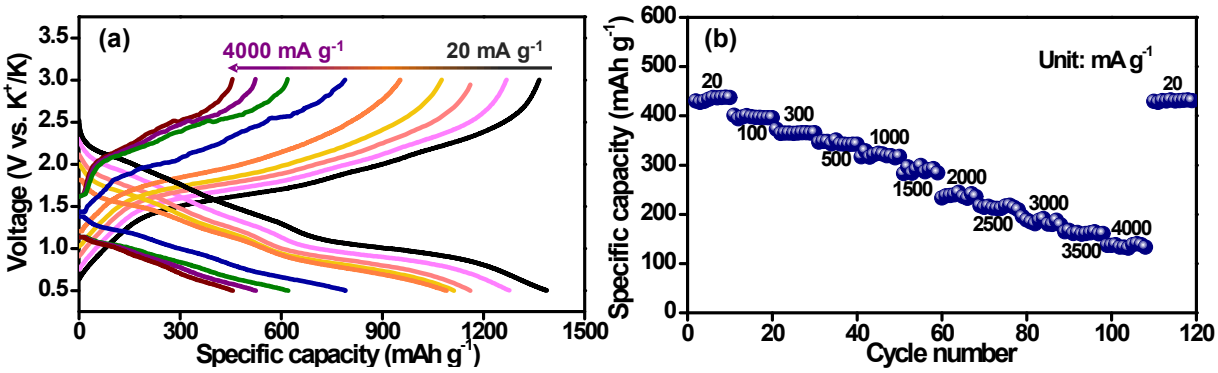

Figure S13. Rate capability of the PCNF/S composite electrode of (a) voltage profiles of Figure 3c, (b) rate performance based on the whole electrode weight.

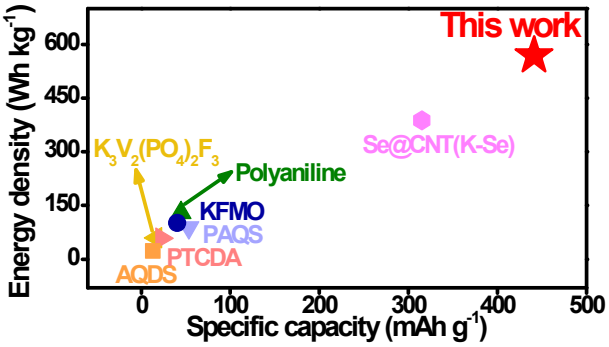

Figure S14. Comparison of energy density of the PCNF/S composite electrode with those of representative reported cathode materials for KIBs in literature.[S1-S7] (Values are taken or estimated from the references and the capacity was calculated based on the whole weight of the electrode, including active materials, conductive agents, binders and current collectors.)

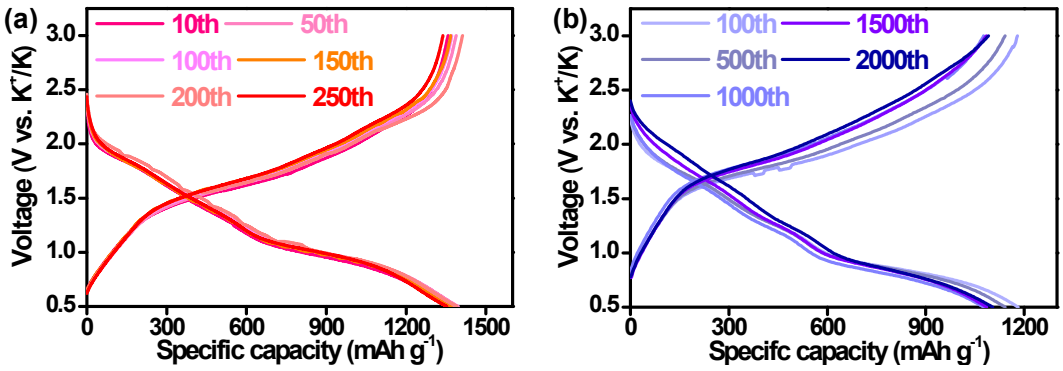

Figure S15. Voltage profiles in selected galvanostatic charge/discharge cycles of the PCNF/S composite electrode of (a) at 20 mA g^{-1} of Figure 3e and (b) at 200 mA g^{-1} of Figure 3f.

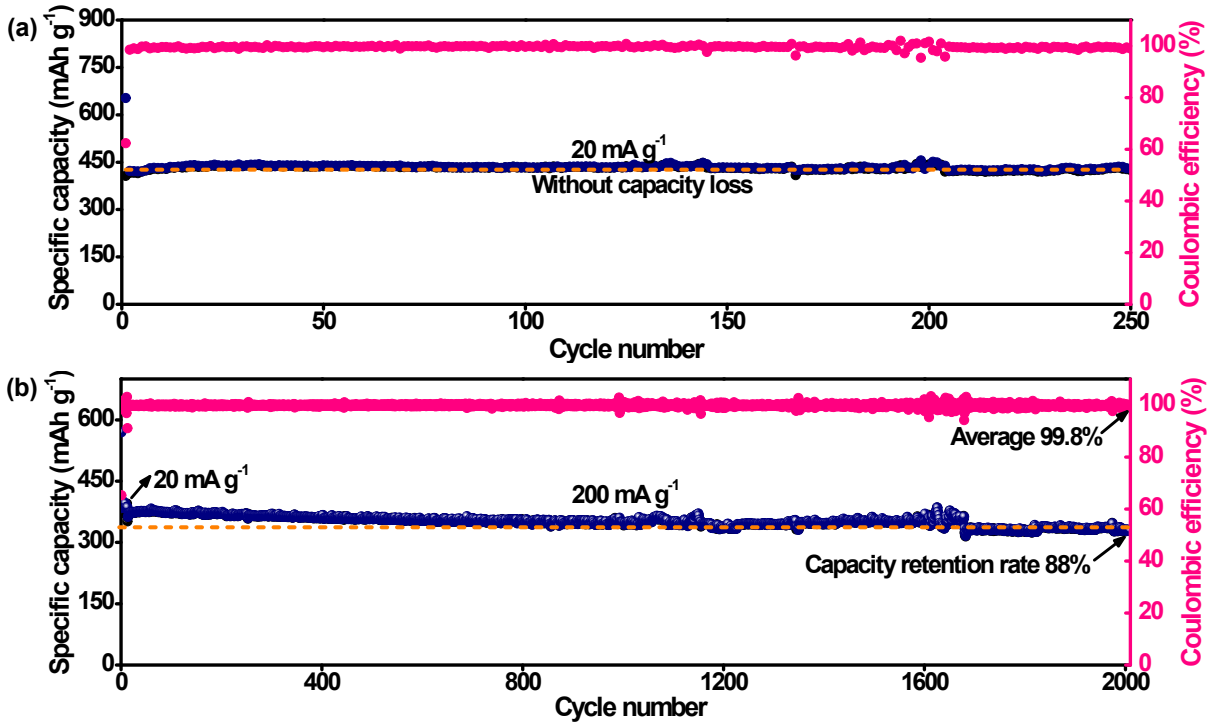

Figure S16. (a) Cycling stability at 20 mA g^{-1} and (d) long-life cycling performance at 200 mA g^{-1} of PCNF/S composite electrode based on the total mass of the composite electrode.

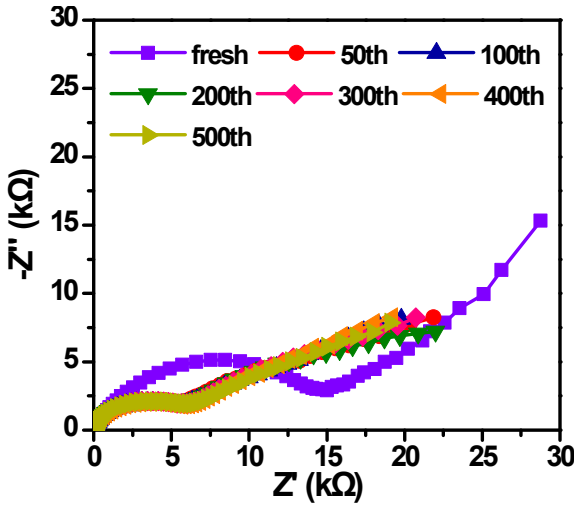

Figure S17. *In-situ* electrochemical impedance spectra evolution of the PCNF/S composite electrode at fresh state and fully depotassiated states with cycling.

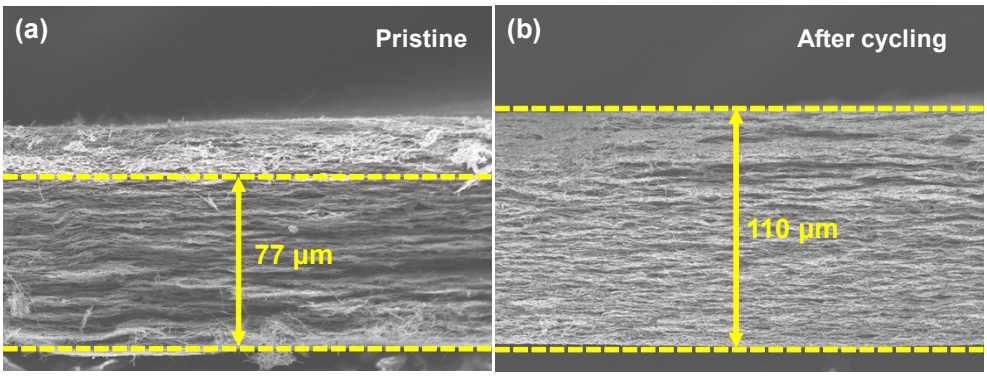

Figure S18. Cross-sectional SEM images of PCNF/S composite electrodes at (a) pristine state and (b) after cycling.

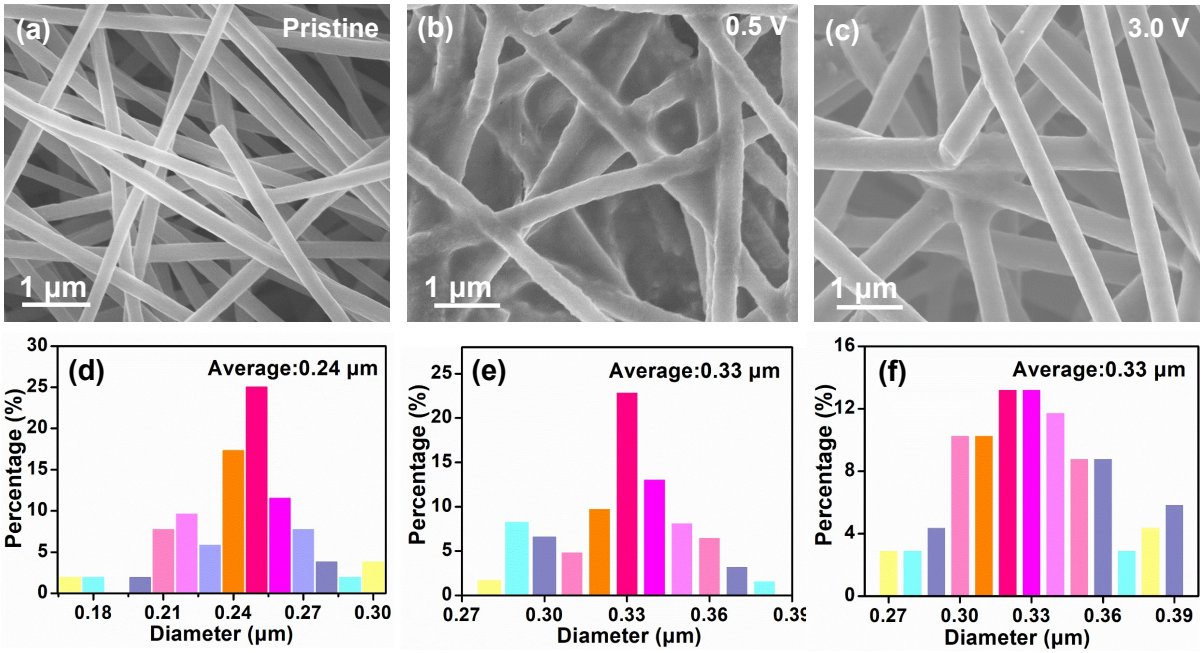

Figure S19. SEM images of the PCNF/S composite electrode at different states: (a) pristine, (b) potassiated to 0.5 V and (c) depotassiated to 3.0 V at the current density of 20 mA g^{-1}, and (d-f) the corresponding diameter distributions.

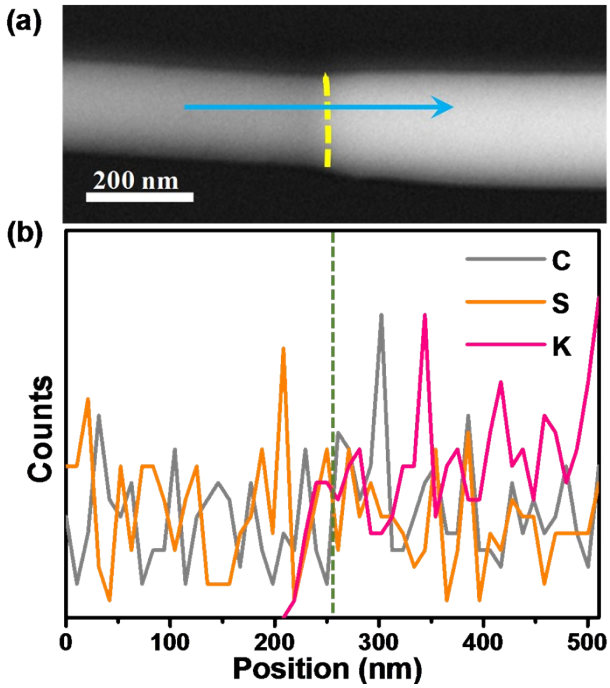

Figure S20. (a) HAADF-STEM image and (b) EDS line-scaning analysis of the PCNF/S composite electrode along with the marked line of blue arrow during the *in-situ* TEM experiment.

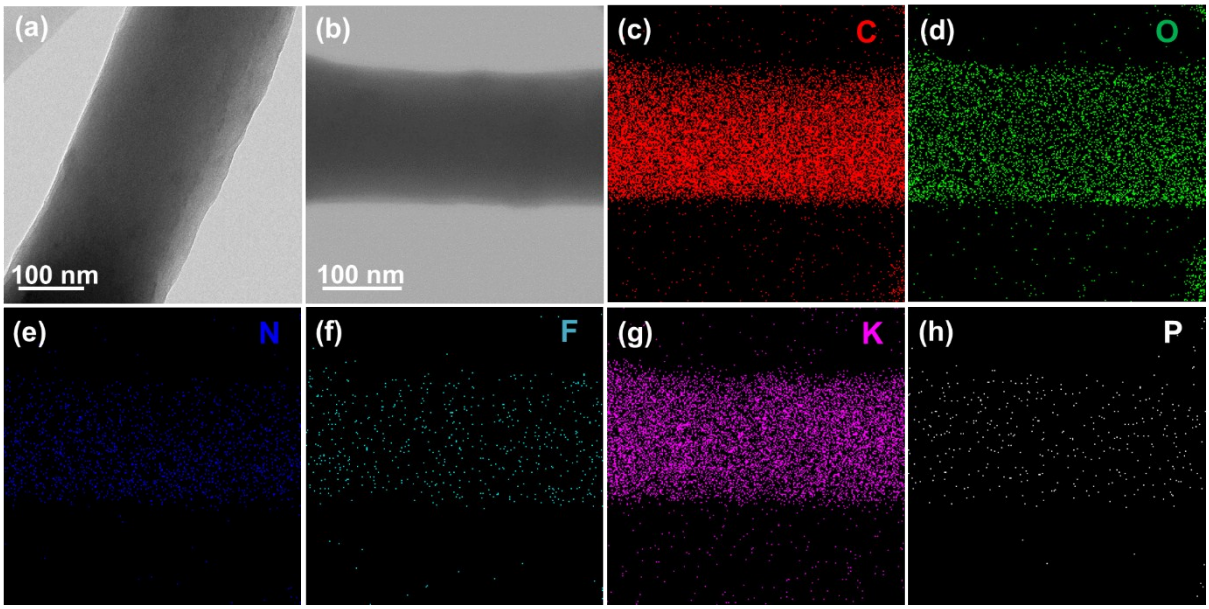

Figure S21. Morphology and structural characterization of the tested PCNF/S composite electrode after 200 cycles at 20 mA g^{-1} with the electrolyte of 0.8 M KPF_6 in EC/DEC: (a) TEM, b) light-field and (c-h) EDS element mapping images of C, O, N, F, K and P, respectively.

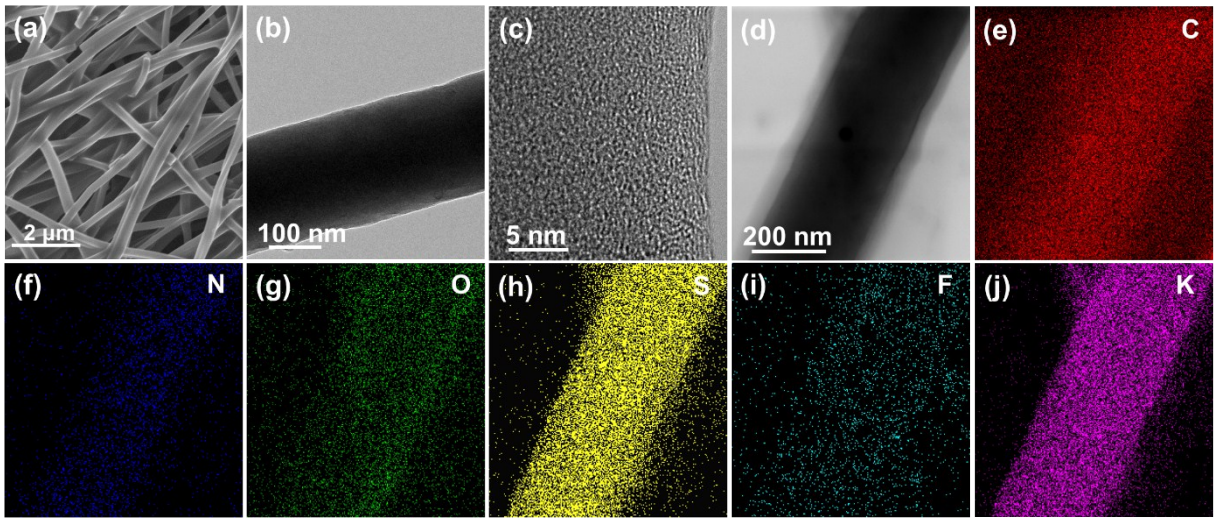

Figure S22. Morphology and structural characterization of the tested PCNF/S composite electrode after 200 cycles at 20 mA g^{-1} with the electrolyte of 1.0 M KFSI in DME: (a) SEM, (b) TEM, (c) HRTEM and (d) light-field and (e-j) EDS elemental mapping images of C, N, O, S, F and K, respectively.

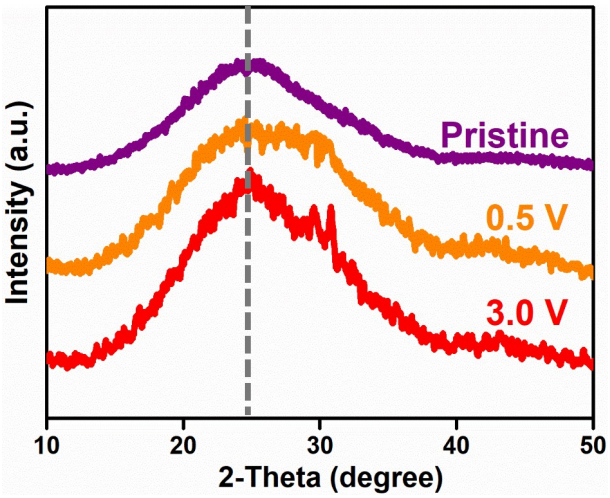

Figure S23. XRD patterns at pristine, potassiated to 0.5 V and depotassiated to 3.0 V states of the PCNF/S composite electrodes at the current density of 20 mA g^{-1} with 1.0 M KFSI in DME.

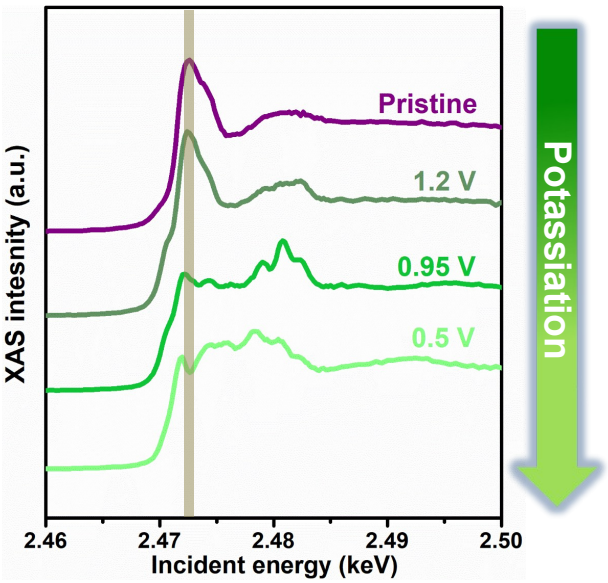

Figure S24. Sulfur K-edge XANES spectra of selected different potassiation states during the first potassiation process of the PCNF/S composite electrode in the electrolyte of 0.8 M KPF_6 in EC/DEC.

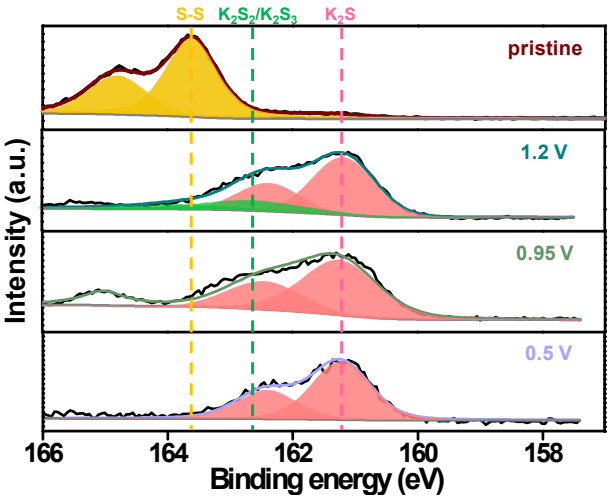

Figure S25. High-resolution XPS spectra of S 2p at different potassiated states during the first potassiation process of the PCNF/S composite electrode in the electrolyte of 0.8 M KPF_6 in EC/DEC.

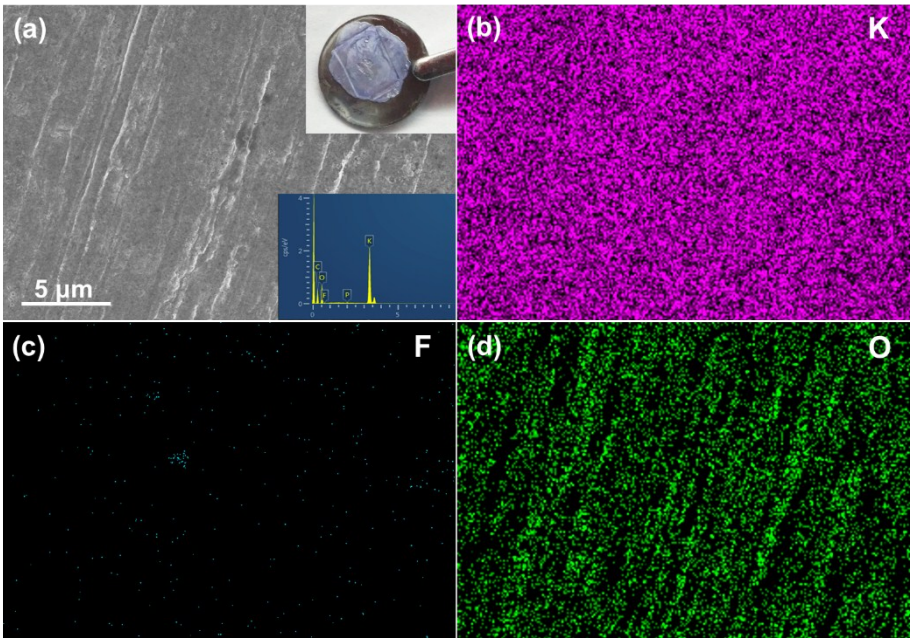

Figure S26. Structural and morphology characterization of the K metal anode after cycling: (a) SEM and (b-d) EDS elemental mapping images of the K metal anodes after 200 cycles at the current density of 20 mA g^{-1} in the electrolyte of 0.8 M KPF_6 in EC/DEC. The insets show the optical photograph and the EDS energy spectrum of the K metal anode.

Table S1. Electrochemical performance comparison of sulfur cathodes in KIBs.

Material	Sulfur content (wt%)	Voltage window (V)	Electrolyte amount (μL)	Sulfur loading (mg cm^{-2})	Cycling (mAh g^{-1}) @cycle life	Capacity retention (%)	Ref.
PCNF/S	**25**	**0.5-3.0**	**50**	**0.5-1**	**1002.4@2000 at 200 mA g^{-1}**	**88**	**This work**
PANI@CMK-3/sulfur	39.2	1.2-2.4	---	---	329.3@50 at 50 mA g^{-1}	63	S8
70S/30CNT	70	1.2-3.0	80	0.478	184@5 at 50 mA g^{-1}	26	S9
K_2S_x catholyte/ 3D-FCN	30	1.2-2.4	50	0.56	376@20 at 55.8 mA g^{-1}	94	S10
SPANs	38	0.8-2.9	---	0.38	387@100 at 125 mA g^{-1}	54	S11
S/CNF	---	1.0-2.8	20	1	600@50 at 114.4 mA g^{-1}	53	S12
CMK-3/S	76	1.2-3.0	---	1.8-2.0	220@10 at 10 mA g^{-1}	36	S13
SPAN (PAA binder)	45.5	0.3-3.0	---	---	450@300 at 837 mA g^{-1}	49	S14
CCS (SPAN)	39.25	0.8-3.0	120	0.39-0.59	672@300 at 150 mA g^{-1}	86	S15
Microporous C/S	18.6	0.5-3.0	---	0.5-1.0	869.9@150 at 20 mA g^{-1}	73	S16
SPAN	39.52	0.5-3.0	---	---	490@100 at 35 mA g^{-1}	95	S17
I-S@pPAN	42	0.8-2.9	246	0.42	388@180 at 1675 mA g^{-1}	54	S18

♣Capacities are calculated based on the mass of sulfur.

Video S1. *In-situ* TEM experiment video during potassiation/depotassiation processes.

Reference

S1. Y. Yao, M. Chen, R. Xu, S. Zeng, H. Yang, S. Ye, F. Liu, X. Wu, Y. Yu, *Adv. Mater.* **2018**, *30*, 1805234.

S2. L. Fan, R. Ma, J. Wang, H. Yang, B. Lu, *Adv. Mater.* **2018**, *30*, 1805486.

S3. B. Li, J. Zhao, Z. Zhang, C. Zhao, P. Sun, P. Bai, J. Yang, Z. Zhou, Y. Xu, *Adv. Funct. Mater.* **2019**, *29*, 1807137.

S4. X. Lin, J. Huang, H. Tan, J. Huang, B. Zhang, *Energy Storage Mater.* **2019**, *16*, 97.

S5. T. Deng, X. Fan, J. Chen, L. Chen, C. Luo, X. Zhou, J. Yang, S. Zheng, C. Wang, *Adv. Funct. Mater.* **2018**, *28*, 1800219.

S6. H. Gao, L. Xue, S. Xin, J. Goodenough, *Angew. Chem. Int. Ed.* **2018**, *57*, 5449.

S7. Z. Jian, Y. Liang, I. Rodríguez-Pérez, Y. Yao, X. Ji, *Electrochem. Commun.* **2016**, *71*, 5.

S8. Q. Zhao, Y. Hu, K. Zhang, J. Chen, *Inorg. Chem.* **2014**, *53*, 9000.

S9. S. Gu, N. Xiao, F. Wu, Y. Bai, C. Wu, Y. Wu, *ACS Energy Lett.* **2018**, *3*, 2858.

S10. J.-Y. Hwang, H.-M. Kim, C. S. Yoon, Y.-K. Sun, *ACS Energy Lett.* **2018**, *3*, 540.

S11. Y. Liu, W. Wang, J. Wang, Y. Zhang, Y. Zhu, Y. Chen, L. Fu, Y. Wu, *Chem. Commun.* **2018**, *54*, 2288.

S12. X. Yu, A. Manthiram, *Energy Storage Mater.* **2018**, *15*, 368.

S13. L. Wang, J. Bao, Q. Liu, C.-F. Sun, *Energy Storage Mater.* **2019**, *18*, 470.

S14. J.-Y. Hwang, H. Kim,; Y.-K. Sun, *J. Mater. Chem. A* **2018**, *6*,14587.

S15. R. Ma, L. Fan, J. Wang, B. Lu, *Electrochim. Acta* **2019**, *293*, 191.

S16. P. Xiong, X. Han, X. Zhao, P. Bai, Y. Liu, J. Sun, Y. Xu, *ACS Nano* **2019**, *13*, 2536.

S17. Y. Zhang, J. Lou, Y. Shuai, K. Chen, X. He, Y. Wang, N. Li, Z. Zhang, F. Gan, *Mater. Lett.* **2019**, *242*, 5.

S18. S. Ma, P. Zuo, H. Zhang, Z. Yu, C. Cui, M. He, G. Yin, *Chem. Commun.* **2019**, *55*, 5267.